SLAC–PUB–4689
July, 1988
E

Polarization at SLC*

MORRIS L. SWARTZ

Stanford Linear Accelerator Center
Stanford University, Stanford, California, 94309

ABSTRACT

The SLAC Linear Collider has been designed to readily accomodate polarized electron beams. Considerable effort has been made to implement a polarized source, a spin rotation system, and a system to monitor the beam polarization. Nearly all major components have been fabricated. At the current time, several source and polarimeter components have been installed. The installation and commissioning of the entire system will take place during available machine shutdown periods as the commissioning of SLC progresses. It is expected that a beam polarization of 45% will be achieved with no loss in luminosity.

Presented at the Workshop on Polarization at LEP
Geneva, Switzerland
November 9-11 1987

* Work supported by the Department of Energy, contract DE–AC03–76SF00515.

1. Introduction

The utility of polarized electron (and positron) beams for the production and study of the Z° boson has been discussed in in many publications[1] and will be discussed in detail at this workshop. It is sufficient to say that the use of polarized beams provides an effective increase in luminosity of one to two orders of magnitude for some standard model measurements and improves the systematic uncertainties associated with those measurements to a level unattainable without polarization. (As an example, the precision of the electroweak mixing parameter $\sin^2\theta_w$ as obtained from a measurement of the left-right polarization asymmetry is compared with that obtained from the forward-backward muon asymmetry in Figure 1.)

In order to exploit these advantages, the SLAC Linear Collider (SLC) has been designed to readily accomodate polarized electron beams. At the current time, nearly all of the additional components that are necessary to produce, accelerate, and monitor the polarized electron beam have been fabricated. It is hoped that the installation and testing of various parts will take place during the coming year. The implementation of the polarized electron beam is not expected to affect the luminosity of the machine in any way. The cost of the entire project is approximately $2 million.

2. The Polarized SLC

A layout of the polarized SLC is shown in Figure 2. The orientation of an electron spin vector is shown as the electron is transported from the electron gun to the interaction point.

A gallium arsenide based photon emission source produces pulses of up to 10^{11} longitudinally polarized electrons at repetition rates of up to 180 Hz. The electrons are then accelerated in the first sector of the linac. The beam pulse achieves an energy of 1.21 GeV as it arrives at the entrance of the LTR (Linac To Ring) transfer line.

The electrons must be stored in the North Damping Ring for one machine cycle (the cycle time is $\geq$ 5.5 ms). A system consisting of the LTR bend magnets and a superconducting solenoid is used to rotate the spins into the vertical direction that is necessary for storage in the damping ring. After one machine cycle, the bunch is extracted and passed through another spin rotation system consisting of the bend magnets of the RTL (Ring-To-Linac) transfer line and two superconducting solenoids. The system is sufficently flexible to provide essentially any spin orientation as the bunch reenters the linac at the beginning of sector 2.

The beam pulse is then accelerated to nearly 50 GeV in the linac. To insure that the spin gymnastics in the damping ring have worked properly and to study many of the potential sources of depolarization, a Møller polarimeter is located at the end of the linac near the PEP injection line. This polarimeter is used primarily for diagnostic purposes.

The beam pulse is then transported through the north machine arc and the final focus section to the interaction point. At full energy, the spin vectors precess roughly 26 times. Vertical precession also occurs in the nonplanar arcs. Since longitudinal polarization is required at the interaction point, the total precession angle must be calculated for the exact machine energy and the polarization at the arc entrance must be adjusted appropriately.

After colliding with the unpolarized positron bunch, the electron beam is transported through the south final focus system where a Compton polarimeter is located. The beam continues to the south extraction line where a second Møller polarimeter is located. The bending magnets of the final focus and extraction line cause an additional spin precession of roughly 540° between the interaction point and the Møller target. Both polarimeters continuously monitor the beam polarization.

3. The Polarized Source

In 1976, Pierce and Meier[2] observed the photoemission of polarized electrons from negative electron affinity gallium arsenide (NEA GaAs). Since then, nearly all polarized electron sources that have been used with accelerators have been based on this technique.[3] These sources have the advantages of relative simplicity, easy reversibility, and good beam characteristics, but are limited to a maximum polarization of fifty percent. The SLC source is an improved version of a GaAs photoemission source that was developed for a previous SLAC experiment.[4] The first part of this chapter describes the physical principles of the source operation and the second part describes the current status of the SLC source.

3.1. Gallium Arsenide Sources

Gallium arsenide is a well-known semiconductor with two very important properties that make it useful as a polarized electron source:

1. Its band structure permits a given spin state to be preferentially pumped into the conduction band.
2. Its surface can be treated to develop a negative work function (hence the term, *negative electron affinity*).

The band structure of GaAs at the energy maximum of the valence band and energy minimum of the conduction band is shown in Figure 3. The band energy versus momentum is shown on the left-hand side and the energy level structure is shown on the right-hand side of the figure. The band gap of the material is $E_g = 1.52\ eV$. At the minimum of the conduction band and the maximum of the valence band, the electron wavefunctions have S and P symmetry, respectively. Spin-orbit splitting causes the $P_{3/2}$ states to reside in energy above the $P_{1/2}$ states by an amount $\Delta = 0.34\ eV$. The absorption of single photons proceeds via an electric dipole transition. The selection rules for the absorption of right-

and left-handed circularly polarized photons are $\Delta m_j = +1$ and $\Delta m_j = -1$, respectively. They are indicated by the solid and dashed arrows in Figure 3. Since the electric dipole operator changes the orbital angular momentum of the inital state by one unit, the spin of the electron remains unchanged in the process.

Let's consider what happens when a right-circularly polarized photon is incident upon a GaAs crystal. The photon direction is the only vector in the system. All angular momentum projections refer to the incident photon direction. If the photon energy E_γ is in the range $E_g \leq E_\gamma \leq E_g + \Delta$, then transitions can only occur from the $P_{3/2}$ states to the $S_{1/2}$ states. Specifically, the P state with $m_j = -3/2$ can make a transition to the S state with $m_j = -1/2$ and the P state with $m_j = -1/2$ can make a transition to the S state with $m_j = +1/2$. In the former case, the emitted electron has spin antiparallel to the incident photon direction (or parallel to its ejected direction). In the latter case, the spin of the emitted electron is parallel to the incident photon direction (antiparallel to its ejected direction). Due to Clebsch-Gordon coefficients (the P state with $m_j = -3/2$ is a pure spin state whereas state with $m_j = -1/2$ is not), the former transition is three times more likely than the latter. The relative transition rates are indicated by circled numbers in Figure 3. This implies that the absorption of a right circularly polarized photon produces a right-handed electron with a polarization

$$P = \frac{3-1}{3+1} = 50\%.$$

Actually, all that's been shown so far is that polarized electrons can be pumped into the conduction band with a beam of circularly polarized photons. In order to make a polarized source, the electrons must leave the material. In normal GaAs, the energy gap from the bottom of the conduction band to the free electron state is approximately 2.5 electron volts. Even with a large applied electric field, pure GaAs is a poor photoemitter. The magic that is necessary to make it an efficient photoemitter is shown in Figure 4. The energy of the various bands is shown as a function of depth near the surface for several materials: pure

GaAs, GaAs with a cesiated-surface, and GaAs with a surface layer of Cs_2O. The energy of the free electron state is shown as E_∞. The addition of cesium to the surface causes the energy gap between the conduction band and the free electron state to decrease to zero. The addition of Cs_2O to the surface causes the gap to become negative! Quantum efficiencies as large as 5% have been been observed for GaAs photocathodes that have been treated with Cs_2O (actually CsF is currently used instead). At photon energies that are appropriate for polarized electron production, quantum efficiencies in the range $0.1\% \rightarrow 0.5\%$ are typical.

In practice, the photoexcited electrons can become depolarized by spin flip scattering processes that occur before emission from the photocathode. Attempts are currently being made to minimize this effect by making very thin photocathodes. The measured electron polarization from several thin photocathodes is presented in Figure 5 for several photon wavelengths. Note that the polarization increases to a value in the range $45\% \rightarrow 50\%$ as the photon energy is decreased to a value near the bandgap of the material. Although the systematic errors of these measurements are typically 10%, electron polarizations near the theoretical maximum are attained.

3.2. The SLC Polarized Source

A drawing of the SLC polarized source is shown in Figure 6. The source is installed on a Y section to facilitate switching from one source to the other. At the current time, the source is installed on the accelerator. Several tests were conducted during the winter 1987-1988 shutdown. A high vacuum bakeout of the Y section was performed. The photocathode was then activated with a CsF treatment. A quantum efficiency of approximately 1% was measured. The vacuum valve that isolates the photoemission gun from the accelerator vacuum was then opened. The lifetime* of the photocathode when exposed to the accelera-

* The photocathode lifetime refers to the decrease in quantum efficiency with time. When the quantum efficiency becomes too low, it can be restored by a CsF activation. The physical photocathode surface is capable of many such reactivation cycles.

tor environment was measured. In the laboratory tests, the cathode lifetime has been measured to be approximately 1000 hours. Unfortunately, the lifetime of the cathode when exposed to the accelerator environment was only 100 hours. The solution to this problem is to improve the accelerator vacuum near the source.

The second major component of the polarized electron source (also shown in Figure 6) is the laser light source. It is a model TFDL-10 flashlamp-pumped dye laser which was built by the Candela Corporation and was extensively modified at SLAC. The laser has been operated with two dyes: oxazine 720 and rhodamine 700. The laser power is shown in Figure 7 as a function of wavelength (which depends upon the dye concentration). The power is the average power at 60 Hz operation. The actual pulse width is 500 ns (full width). Also shown in Figure 7 is the expected electron polarization for each photon wavelength. It is clear that the rhodamine dye produces more power in the long wavelength region that is desirable for high polarization.

Unfortunately, this is only part of the story. The dyes are gradually destroyed by exposure to the high intensity illumination of the flash lamps. The lifetime of each dye determines the frequency of laser maintainance that is necessary in actual operations. At 60 Hz operation, the lifetimes of the oxazine and rhodamine dyes have been measured to be 216 hours and 41 hours, respectively. The operational maintenance interval is determined by a number of parameters. If one assumes that the cathode lifetime is 100 hours and that the initial quantum efficiency is 1%, then the production of 10^{11} electrons at 120 Hz would require source maintenance each 8.3 days with the oxazine dye and each 2.9 days with the rhodamine dye. The rhodamine dye is capable of producing higher polarization but requires more frequent maintenance. In either case, the situation is tolerable but not entirely satisfactory. There are plans to investigate more dyes in the near future.

The time structure of the laser pulse differs substantially from the required time structure of the electron pulses. Each machine cycle, the SLC source must

produce two two-nanosecond electron pulses that are separated in time by 60 ns. The solution to the problem is to modulate the the 500 ns laser pulse with the apparatus that is shown in Figure 8. The photon beam emerges from the laser and passes through a double prism to insure 100% linear polarization. It is then passed through a Pockels cell, a second double prism, and a second Pockels cell. The *fast* and *slow* axes of the Pockels cells are rotated by 45° with respect to the polarization direction of the beam. The polarizing axis of the second prism is rotated by 90° with respect to the first prism. In the absence of a voltage applied to the first Pockels cell, no light is transmitted through the system. The laser pulse is modulated by applying a high voltage signal to the first Pockels cell that has the correct time structure (two 2-ns pulses that are separated by 60 ns). The amplitude of the voltage is adjusted to produce a phase shift of 180° between the axes of the cell. This causes the polarization vector of the beam to rotate by 90°. The beam is thus fully transmitted through the second prism for the duration of the high voltage pulse and the correct time structure is established. The voltage applied to the second Pockels cell is held constant for the duration of the machine cycle and is adjusted to produce a 90° phase shift between the fast and slow axes. The system therefore transmits either right- or left-circularly polarized photons (depending upon the sign of the voltage).

4. The Spin Rotation System

The second major element of the polarized SLC is the spin rotation system. As was mentioned in Chapter 2, the spin rotation system has two functions:

1. To rotate the (initially longitudinal) polarization vector of the electron bunch into the vertical direction for storage in the North Damping Ring.

2. To allow the orientation of the electron polarization vector to be controlled as the bunch reenters sector 2 of the linac. This is necessary to compensate for precession in the machine arcs.

A detailed representation of the north damping ring, the north LTR transfer line, and the north RTL transfer line is shown in Figure 9. The orientation of the polarization vector at various places is shown by the double arrow. The electron bunch arrives at the entrance to the LTR transfer line with an energy of 1.21 GeV. At this energy, the spins precess by 90° for each 32.8° that the electron trajectories are bent by a transverse magnetic field. The initial bend angle of the LTR has been chosen to be $5 \times 32.8°$. The longitudinal polarization of the beam emerging from sector 1 of the linac is therefore rotated into the horizontal direction. A superconducting solenoid of strength 6.34 T-m is introduced into the LTR optics after the first bend. The solenoid has only a small effect on the optics of the transport system but causes a rotation of the spin vector about the beam axis by 90°. The spins are therefore rotated into the vertical (either upward or downward) direction. After one machine cycle ($\geq$ 5.5 ms), the electron bunch is extracted from the damping ring with a horizontal kicker magnet and passed through a second superconducting solenoid magnet. The horizontal bend magnets of the RTL transfer line then deflect the beam by an angle of $3 \times 32.8°$ before it reenters the linac at the beginning of sector 2. A third superconducting solenoid is introduced into the linac lattice just downstream of the reentry point. If the second (RTL) solenoid is adjusted to have the same strength as the first (LTR) solenoid has, the system will restore the longitudinal beam polarization. If it is not energized, the beam polarization will be vertical upon reentry into the linac. The third (linac) solenoid can then rotate the polarization vector to any transverse orientation. The combination of the two solenoids and the RTL bending magnets permits the selection of any orientation of the polarization vector.

Status of the Spin Rotation System

At the current time, all three spin rotation solenoids have been fabricated and delivered to SLAC. The magnets and their cryogenic and control systems have been assembled in a large test facility at SLAC. The entire system is undergoing

extensive testing. The installation of the spin rotator solenoids into the LTR and RTL transport lines requires relatively minor changes to the optics and instrumentation of the beam lines. The installation of the solenoid into sector 2 of the linac is somewhat more involved. A single accelerator section must be removed (which results in a loss of 50 MeV of energy to the electron beam). Three quadrupole magnets must be moved and two others must be installed.

5. Polarimetry at SLC

The polarization of the SLC electron beam will be monitored by three polarimeters. Two of the polarimeters are based upon polarized Møller scattering. They provide three-axis polarimetry and have moderate precision ($\delta P/P \lesssim 5\%$). The third polarimeter is based upon polarized Compton scattering and can provide high precision ($\delta P/P \approx 1\%$) measurements of the longitudinal beam polarization. The Møller polarimeters are located at the end of the linac and in the south extraction line. The Compton polarimeter is located at the last bend magnet of the south final focus.

5.1. The Møller Polarimeters

The Møller polarimeters make use of the polarized asymmetries of the cross section for electron-electron elastic scattering. At tree level, the differential cross section for this process in the center-of-mass frame (in the $m_e \to 0$ limit) is given by the following expression

$$\frac{d\sigma}{d\Omega} = \frac{\alpha^2}{s}\frac{(3+\cos^2\theta)^2}{\sin^4\theta}\Big\{1 - P_z^1 P_z^2 A_z(\theta) - P_t^1 P_t^2 A_t(\theta)\cos(2\phi - \phi_1 - \phi_2)\Big\}$$

where: s is the square of the total energy in the cm frame; θ is the cm frame scattering angle; ϕ is the azimuth of the scattered electron (the definition of $\phi = 0$ is arbitrary); P_z^1, P_z^2 are the longitudinal polarizations of the beam and target, respectively; P_t^1, P_t^2 are the transverse polarizations of the beam and target,

respectively; ϕ_1, ϕ_2 are the azimuths of the transverse polarization vectors; and $A_z(\theta)$ and $A_t(\theta)$ are the longitudinal and transverse asymmetry functions which are defined as

$$A_z(\theta) = \frac{(7+\cos^2\theta)\sin^2\theta}{(3+\cos^2\theta)^2}$$

$$A_t(\theta) = \frac{\sin^4\theta}{(3+\cos^2\theta)^2.}$$

The differential cross section is the product of the unpolarized cross section and the sum of one and two polarization dependent terms. The first is the product of the longitudinal polarizations of the beam and target particles and the function $A_z(\theta)$. The second is the product of the transverse polarizations of the two electrons, an azimuthal factor, and the function $A_t(\theta)$. The unpolarized cross section, $A_z(\theta)$, and $A_t(\theta)$ are plotted as functions of $\cos\theta$ in Figure 10. Both asymmetry functions are maximal for 90° scattering. The longitudinal asymmetry function becomes quite large ($A_z(90°) = 7/9$) whereas the transverse asymmetry function never exceeds 1/9. The analyzing power of any polarimeter scales as the product of the unpolarized cross section and the square of the asymmetry. This combination is also largest at $\theta = 90°$ but has a rather broad maximum.

The laboratory momentum and angle of the scattered electron, P' and θ_{lab} are related to the center-of-mass frame scattering angle by the following expressions,

$$P' = \frac{P}{2}[1+\cos\theta]$$

$$\theta_{lab} = 2m_e\left[\frac{1}{P'} - \frac{1}{P}\right]$$

where P is the momentum of the incident electron and where m_e is the mass of the electron. The extraction line polarimeter has been designed to accept an interval of momentum $\Delta P'/P' = \pm 5\%$ about $P' = P/2$. Its acceptance is therefore centered about $\theta = 90°$. The linac polarimeter makes use of the first bend magnet of the PEP injection line as an analyzing element. The PEP injection line cannot transport electron momenta larger than 15 GeV/c. At a

beam energy of 46 GeV, this corresponds to a minimum center-of-mass angle of 110°. The corresponding laboratory angles, unpolarized cross sections, and polarization asymmetries are summarized in Table I below:

Table I

The accepted cm and laboratory angles, cross section, longitudinal asymmetry and transverse asymmetry for the linac and extraction line Møller polarimeters. The beam energy is assumed to be 46 GeV. The cross sections are given in units of α^2/s.

Polarimeter	θ	θ_{lab}(mRad)	$d\sigma/d\Omega$	A_z	A_t
Linac	110°	6.8	12.5	0.64	0.08
Extraction Line	90°	4.7	9.0	0.78	0.11

The larger scattering angle regime accepted by the linac polarimeter reduces the analyzing power only slightly (by 6%) as compared with the extraction line device.

Polarimeter Design

It is clear that the electron beam polarization can be monitored by providing a target containing polarized electrons and by measuring the asymmetry of the cross section caused by reversing either the beam or target polarizations. The beam polarization P_b is then related to the measured asymmetry A_{exp} by the following simple expression

$$P_b = \frac{A_{exp}}{P_{tgt} A_{theor}}$$

where P_{tgt} is the target polarization and A_{theor} is the theoretical longitudinal or transverse asymmetry given above. A diagram of the extraction line polarimeter is shown in Figure 12. Note that the horizontal bending magnets have no function for the polarimeter (they make synchrotron radiation for the SLC energy spectrometer and background for the polarimeter). The linac polarimeter differs only in the choice of analyzing magnet and detector. The main elements of both polarimeters are:

1. A magnetized foil target.

2. A collimator to define a scattering plane (defines the azimuth of the scattered particles).

3. A magnet and aperture that select the momentum range to be accepted (which is equivalent to selecting the cm scattering angle). Note that the bending plane of the magnet is perpendicular to the scattering plane defined by the collimator. This is done to decouple P' from θ_{lab}.

4. A detector that is capable of measuring the electron rate as a function of position. A shower counter sampled with very small (2 mm diameter) proportional tubes is used in the extraction line. The linac polarimeter uses a silicon strip detector.

The counting rates in both polarimeters are in the range $50 \rightarrow 100$ electrons per pulse. It is therefore expected that longitudinal polarization measurements will require $1 \rightarrow 2$ minutes to achieve a statistical precision of 5%. Transverse polarization measurements will require roughly one hour to achieve the same precision.

Møller Target

A single polarized target design has been used for both polarimeter targets. A *beam's eye view* of the target assembly is shown in Figure 11. A holder containing four iron foils can be moved through the beam. Two foils are transverse to the beam axis and two are tilted at an angle of 20° with respect to the beam axis. A three sets of interleaved Hemholz can produce a 100 gauss magnetic field along any of the three axes. This field is sufficient to magnetically saturate a foil along its axis. At saturation, the spins of two of the 26 valence electrons are (anti)aligned with the external field (the maximum polarization is therefore 8%). The actual target polarization is measured by the following procedure:

1. A small pickup coil is placed around the target foil.

2. The direction of the driving field is reversed and the induced coil voltage is measured.

3. The target is removed from within the pickup coil and step 2 is repeated.

Step 2 measures the total B field induced within the foil. Step 3 measures just the driving H field. The difference between the measurements determines the magnetization density of the foil. The magnetization density is closely related to the target polarization (it must be corrected for orbital effects).[6]

Backgrounds

The Møller scattering signal that was measured in the polarimeter of the SLAC polarized electron-deuteron scattering experiment[4] is shown in Figure 13. The number of detected electrons is shown as a a function of scattering angle (the upper plot). The signal consists of a smoothly varying distribution and a peak. The Møller scattering peak occurs at the angle which corresponds to the accepted momentum (according to the electron-electron two body kinematics). The continuous distribution provides a 15 $\rightarrow$ 20% background to the Møller signal. Both the shape and the magnitude of the background are well described by the process $e^- + N \rightarrow e^- + N + \gamma$ (also known as the Bethe-Heitler process).[7] A similar background is expected to be present in the extraction line polarimeter. The larger angle regime accepted by the linac polarimeter is expected to be less contaminated by background (by a factor of 2-3).

Systematic Errors

The ability to operate the polarimeters in four polarization modes (two beam polarization directions $\times$ two target polarization directions) will help to study many systematic problems. Nevertheless, it is expected that the precision that can be achieved will be limited by the following systematic effects:

1. The target polarization can be measured with a precision of two or three percent. Better precision probably requires a good understanding of the shape of the magnetization density distribution within the target.

2. The uncertainty in the subtraction of the intrinsic background will probably be less two percent.

3. A complete set of radiative corrections for polarized Møller scattering has not been calculated. The effect on the size of the cross section is quite large (of order 20%). The effect on the asymmetry is estimated to be quite small (less than 1%).

4. The measurement of an asymmetry is sensitive to the linearity of the detector. The non-linearities can probably be corrected and controlled to less than one percent.

5. The passage of the beam through the target can disrupt the spin alignment of the electrons. At SLC, the effect is estimated to be less than a one percent uncertainty on the target polarization.

The combined effect of the above uncertainties is less than 5%. It appears that with a bit of care and good luck, the systematic error could be controlled to $2 \rightarrow 3\%$.

Status of the Møller Polarimeters

At the current time, all components of both polarimeters have been fabricated. The linac polarimeter target assembly has been calibrated and installed. A number of background studies have been conducted with a prototype silicon detector. The extraction line polarimeter target assembly and collimator will be installed during the next extended shutdown of the machine. The lead-proportional tube detector will be installed in the near future and background studies will be conducted.

5.2. THE COMPTON POLARIMETER

The Compton polarimeter makes use of the large polarization asymmetry in the cross section for elastic electron-photon scattering. The light source initially will be a frequency doubled Nd:YAG laser which produces 2.23 eV photons (a later upgrade to an excimer laser is being considered). The kinematics of the scattering of optical photons with high energy electrons in the laboratory frame are discussed first. After the variables have been defined, the polarized cross section is presented.

Compton Scattering Kinematics

The kinematical properties of the scattering of a high energy electron with an optical photon seem quite strange to those accustomed to working in reference frames that are nearer the center-of-mass frame. The energy of the electron is typically 10 orders of magnitude larger than that of the photon. It is clear that all final state particles are swept into the forward direction (along the incident electron direction). It is therefore convenient to define all angles with respect to the incident electron direction. The direction of the outgoing photon, θ_K, differs from the normal definition of the scattering angle by 180° (if the colliding e-γ are collinear). Let E, E', K, and K' be the incident electron energy, scattered electron energy, incident photon energy, and scattered photon energy, respectively. The maximum energy of the scattered photon K'_{max} and the minimum energy of the scattered electron E'_{min} can then be written as

$$K'_{max} = E(1-y)$$
$$E'_{min} = Ey$$

where the parameter y is defined as

$$y \equiv \left(1 + \frac{4EK}{m^2}\right)^{-1}.$$

The emission angle of the scattered photon θ_K is related to the scattered photon

energy by the following expression,

$$K' = K'_{max}\left[1 + y\left(\frac{E\theta_K}{m}\right)^2\right]^{-1}$$
$$= K'_{max} \cdot x$$

where the definition of x is obvious. The parameter x varies from unity at zero emission angle to zero at larger angles. The scale of the angular range is set by the angle for which the energy has been reduced by a factor of two. This occurs when $E\theta_K\sqrt{y}/m = 1$ or at the angle $\theta_K = m/E\sqrt{y}$. For the SLC Compton polarimeter operating with a 46 GeV beam, the value of the parameter y is 0.389. Therefore, the maximum photon energy is 28.1 GeV and the minimum electron energy is 17.9 GeV. The angle at which the photon energy has been decreased by a factor of two is 1.8×10^{-5} radians. The scattered electron and photon both remain along the beam direction.

The Polarized Cross Section in the Laboratory Frame

The polarized cross section can be expressed in terms of the laboratory variables x, y, and the azimuth of the photon with respect to the electron transverse polarization ϕ as follows,[8]

$$\left(\frac{d^2\sigma}{dxd\phi}\right)_{Compton} = \left(\frac{d^2\sigma}{dxd\phi}\right)_{unpol}\left\{1 - \mathcal{P}^\gamma\left[\mathcal{P}_z^e A_z^{e\gamma}(x) + \mathcal{P}_t^e \cos\phi A_t^{e\gamma}(x)\right]\right\}$$

where: the unpolarized cross section is defined as

$$\left(\frac{d^2\sigma}{dxd\phi}\right)_{unpol} = r_\circ^2 y\left\{\frac{x^2(1-y)^2}{1-x(1-y)} + 1 + \left[\frac{1-x(1+y)}{1-x(1-y)}\right]^2\right\};$$

$\mathcal{P}_z$, $\mathcal{P}_t$ are the longitudinal and transverse polarizations of the electron; $\mathcal{P}^\gamma$ is the *circular* polarization of the photon; and where the longitudinal and transverse

asymmetries are defined as

$$A_z^{e\gamma}(x) = r_\circ^2 y[1 - x(1+y)]\left\{1 - \frac{1}{[1-x(1-y)]^2}\right\} \cdot \left(\frac{d^2\sigma}{dxd\phi}\right)^{-1}_{unpol}$$

$$A_t^{e\gamma}(x) = r_\circ^2 yx(1-y)\frac{[4xy(1-x)]^{1/2}}{1-x(1-y)} \cdot \left(\frac{d^2\sigma}{dxd\phi}\right)^{-1}_{unpol}$$

These equations are difficult to visualize and interpret without a bit of assistance. The unpolarized cross section and the longitudinal and transverse asymmetries are plotted as functions of x in Figure 14 for $y = 0.389$. The unpolarized cross section is very large (several hundred millibarns) and peaked at $x = 1$. The longitudinal asymmetry has a maximum of 75% also at $x = 1$. Note, however, that as x is decreased, $A_z^{e\gamma}$ decreases rapidly and becomes negative near $x = 0.72$. It reaches a minimum of -25% near $x = 0.47$ and returns to zero at $x = 0$. The transverse asymmetry is zero at both endpoints and reaches a maximum of 33% near $x = 0.75$.

Polarimeter Design

The location of the SLC Compton polarimeter is shown in Figure 15. The laser is brought into collision with the electron beam after it has passed through and immediately before it enters the first bend magnets of the final focus region. Since no precession occurs between the interaction point and the Compton collision point, it is sufficient to measure only the longitudinal component of the electron polarization. As is shown in Figure 14, the largest cross section and largest longitudinal asymmetry occur near $x = 1$. Since both quantities are very sensitive to the precise value of x (or alternatively, energy), there is a clear advantage in measuring the scattered electrons. The electrons can be momentum analyzed rather precisely in large numbers. The main elements of the polarimeter are as follows:

1. The pulsed laser. As was stated previously, the polarimeter will initially use a frquency doubled Nd:YAG laser operating at 4 millijoules per pulse. The pulse length is 8 nanoseconds and the repetition rate is 15 Hz.

2. The laser optics and light path. The beam is circularly polarized with a Pockels cell and transported to a collision point that is approximately 12 m downstream of the SLC interaction point. The beam size at the collsion point is 1.2 mm and the crossing angle is 20 milliradians.

3. The analyzing magnet is the first bending magnet of the final focus region. The endpoint (17.9 GeV) electrons are deflected by approximately 15 milliradians with respect to the unscattered beam.

4. The detector is a multicell gas Cerenkov counter that has a threshold energy of 20 MeV. It is located approximately 3 m downstream of the magnet center.

The counting rate is expected to be approximately 190 events per machine pulse. Because the laser target has essentially 100% polarization (as compared with the Møller target polarization of 8%), many fewer counts are required to achieve a given statistical precision than are required for the Møller polarimeters. It is expected that a 1% statistical precision can be achieved in a 70 second run.

Backgrounds

While Compton polarimeters have do not have the intrinsic backgrounds of the Møller technique, they can have serious background problems. The electron-positron collisions produce low energy electrons that are collinear with the beam axis via the process $e^+e^- \rightarrow e^+e^-\gamma$. This background decreases as the energy of the accepted electrons is decreased. For electron energies below 25 GeV, it is expected to be less than 15% of the signal. A second and potentially more serious background is the off-energy beam halo that is produced by the scattering of the beam tails from various apertures. Linear collider experiments are affected much more by this type of problem than storage ring experiments are. It is difficult even to estimate the size of this background since it depends upon machine parameters that are not measured well and upon details of the precise machine tune.

Both types of background are directly measureable by turning off the laser

for machine pulses. They can be therefore be tolerated to fairly high levels.

Systematic Errors

The list of possible systematic errors that apply to the Compton polarimeter is very similar to that given the Møller section:

1. As with Møller scattering, it is essential to understand the degree of polarization of the target. Although the laser beam must be passed through windows and reflected from mirrors, it appears that the uncertainty on the beam polarization can be controlled to $\Delta P^{\gamma}/P^{\gamma} \lesssim 1\%$.

2. Unless the machine related backgrounds are very severe, it appears that they and the radiative Bhabha background can be measured and subtracted from the total signal. The effect on the measured asymmetry can be kept to a few tenths of one percent.

3. A complete set of first order radiative corrections to polarized Compton scattering has been calculated by Gongora and Stuart.[9] The theoretical uncertainty on the longitudinal asymmetry is certainly small as compared with the other systematic errors discussed in this section.

4. As with the Møller case, it is essential to monitor non-linearities of the detection system. Most detection systems are not linear to better than a percent or several percent. It appears that these can be corrected to the level of a few tenths of one percent.

5. Since the longitudinal asymmetry is a strong function of the scattered particle momentum, it is very important to understand the energy scale of the detector. At $y = 0.389$, an energy shift of 100 MeV causes a fractional change in the asymmetry of 1.1 %. A good energy calibration can be derived from endpoint of the scattered electron energy distribution. Since the scattering cross section is largest at the endpoint, it should be relatively straightforward to observe. This does require good spatial resolution of the detector (less than a few hundred microns).

With some care, it appears that the total systematic uncertainty can be controlled to the one percent level.

Status of the Compton Polarimeter

At the current time, the laser light path has been partially installed. The laser has been operated successfully for many years as part of the SLAC backscattered photon beam. A prototype gas Cerenkov cell has been installed downstream of the analyzing magnet. Background studies are being conducted in an attempt to measure the machine luminosity via the radiative Bhabha process.

6. Depolarization Effects

There are numerous possible sources of electron beam depolarization. None of them are expected to be serious. The following is a summary of the most important.

6.1. Depolarization in the Linac

The depolarization of a longitudinally polarized electron beam by the SLAC linac has been calculated to be very small.[10] This has been verified by several experiments.[11,4] The polarized SLC does differ in two respects from the old SLAC linac:

1. The electron bunches are much smaller than they were for the fixed target experiments. It was pointed out by W.K.H. Panofsky[12] that the intra-bunch fields could depolarize the bunch via an effect that is analogous to Thomas precession. More detailed calculations indicate that this effect causes less than a one percent depolarization of the beam.

2. The SLC must accelerate beams with transverse components of the polarization vector. This is not expected to be a problem, however, detailed calculations and experimental verification are still needed.

6.2. Depolarization in the Damping Ring

Since the helicity of each electron pulse is determined by a random number generator at the source, half of the electron pulses stored in the north damping ring will have their polarization vectors aligned with the guide field and half will have anti-aligned polarization vectors. The natural polarization of a storage ring by the Sokolov-Ternov effect[13] causes the spins to anti-align themselves with the guide field. This would cause the depolarization of the aligned bunches if they were stored in the ring for an appreciable fraction of a polarizing time. The polarizing time for the damping ring is approximately 15 minutes. Since the storage time of an electron bunch is only 8 milliseconds (at a 120 Hz repetition rate), this effect is negligable. Indeed, the short storage time (which is several damping times) implies that the only process that could cause a serious problem is resonant depolarization. The resonance condition is

$$\nu = N + I\nu_x + J\nu_y + K\nu_s$$

where: ν is the spin tune of the damping ring (the number of spin precessions per orbit); N, I, J, K are integers; ν_x and ν_y are the horizontal and vertical betatron tunes, respectively; and ν_s is the synchrotron tune of the damping ring. The SLC damping ring is designed to operate at an energy $E = 1.21$ GeV. The spin tune at this energy is given by the expression

$$\nu = \frac{g-2}{2} \cdot \frac{E}{m_e} = \frac{E}{440.65 \text{ MeV}} = 2.746$$

(where $(g-2)/2$ is anomalous magnetic moment of the electron). The horizontal and vertical betatron tunes are $\nu_x = 7.20$ and $\nu_y = 3.20$, respectively (the $\nu_x - \nu_y = 4$ coupling resonance is used to produce round beams). The synchrotron tune is very small ($\nu_s \simeq 0.04$). Therefore, the nearest spin depolarizating resonance occurs when $N, I, J = 6, 0, -1$ (the synchrotron tune is ignored since only relatively weak resonances are associated with it). The right hand side

of the resonance equation is equal to 2.80 in this case. Since the natural width of this sideband resonace is expected to be less than 0.001, no serious resonant depolarization is expected.

6.3. Depolarization in the Arcs

The SLC arcs are fairly achromatic transport systems (they can transport a momentum interval $\Delta P/P = 5\%$). Since the total precession angle is a sensitive function of the beam energy, the finite energy spread of the beam ($\Delta P/P = 0.2\%$) causes a spread in the final spin directions of the electrons. The average longitudinal polarization at the interaction point is reduced by 2.2%.

6.4. Depolarization from Beam-Beam Interactions

Because the SLC beams are very small at the interaction point, each beam is subjected to very strong electromagnetic fields during the collision. These fields cause some depolarization of the electron bunch. The size of the effect is given by the expression

$$\Delta\theta_s = \frac{g-2}{2} \cdot \frac{E}{m_e} \cdot \theta_d$$

where: $\Delta\theta_s$ is the average precession angle of beam particles; E is the beam energy; and θ_d is the disruption angle of the beam. Since the disruption angle at SLC is roughly one milliradian, the average depolarization is less than one percent.

6.5. Systematic Effects

It is possible that the average beam polarization as measured by the two downstream polarimeters be different from the luminosity weighted average polarization. There are two possible causes for this effect.

1. The beam-beam interaction obviously changes the polarization before it arrives at the Compton and extraction line Møller polarimeters. The size of this effect is estimated to be less than 0.5%.

2. If the electron beam at the interaction point has a non-zero dispersion function, it is possible that a beam-beam targeting error could cause the luminosity weighted beam energy and polarization to differ from the average beam energy and polarization. The beam-beam deflection process allows the beam to be targeted to within a small fraction of the beam sizes. Therefore, even if the dispersion function at the interaction point were as large as 3 mm (which is quite large), the fractional deviation of the monitored polarization from the average one is less than two percent. If the dispersion function is the more normal 1 mm, this effect is a few tenths of one percent.

7. Summary

Polarized beams can rather naturally be incorporated into a linear collider like SLC. Although some care is required, there are no technical reasons that make the machine difficult to polarize. Since the polarized electron source is capable of performing as well as the normal unpolarized thermionic source, no degradation in machine performance is expected to result from the implementation of polarized beams. The hardware for producing, accelerating, and monitoring a polarized electron beam in SLC is in a reasonably advanced state of preparation. The installation schedule is being determined almost entirely by the rate of progress in commissioning the machine.

Acknowledgements:

This document has benefited in both form and and content by the scrutiny of Ken Moffeit.

REFERENCES

1. A complete list of every publication that has discussed this topic would be huge. The following is just a sample of those that discuss the most basic asymmetries: *Proceedings of the LEP Summer Study at Les Houches, 1978* CERN 79-01 (1979); C.Y. Prescott, SLAC PUB 3120 (1983); *Physics at LEP*, edited by J. Ellis and R. Peccei, CERN 86-02 (February 1986); B.W. Lynn and C. Verzegnassi, *Physical Review* **D35**, 3326 (1987); A. Blondel, B.W. Lynn, F.M. Renard, and C. Verzegnassi, Montpellier preprint PM/87-14 (March 1987).

2. D.T. Pierce and F. Meier, *Physical Review* **B13**, 5484 (1976).

3. A nice review of low energy polarized electron sources is C.K. Sinclair, SLAC-PUB-3505, November 1984. Also published in *Proceedings of the* 6^{th} *International Symposium on High Energy Spin Physics, Marseille France*, edited by J. Soffer, Les Editions de Physique, Les Ulis France, 1985.

4. C.Y. Prescott et al., *Physics Letters* **B77**, 347 (1978).

5. S.F. Alvarado et al., *Zeitschrift für Physik* **B44**, 255 (1981).

6. For more details, see the article by H. Frauenfelder and A. Rossi, Vol. 5, Part B, pg 243 of *Methods of Experimental Physics*, edited by I.C.L. Yuan and C.S. Wu, Academic Press, New York, 1963.

7. H. Bethe and W. Heitler, *Proceedings of the Royal Society A* **146**, 83 (1934).

8. C.Y. Prescott, SLAC-TN-73-1, January 1973.

9. A. Gongora and R.G. Stuart, Max Plank Institute preprint MPI-PAE/PTh-55/87, July 1987.

10. R.H. Helm and W.P. Lysenko, SLAC-TN-72-1 (March 1972) and M.J. Alguard et al., *Nuclear Intruments and Methods* **163**, 29 (1979).

11. P.S. Cooper et al., *Physical Review Letters* **34**, 1589 (1975); M. J. Alguard et al., *Physical Review Letters* **37**, 1258 and 1261 (1976); M. J. Alguard et al., *Physical Review Letters* **41**, 70 (1978); and W.B. Atwood et al., *Physical Review* **D18**, 2233 (1978).

12. W.K.H. Panofsky, SLAC-CN-361, (August 1987).

13. A.A. Sokolov and I.M. Ternov, *Soviet Physics-Dolkady* **8**, 1203 (1964).

FIGURE CAPTIONS

1) The expected uncertainty of a measurement of the left-right asymmetry A_{LR} as a function of the number of events used. The beam polarization is taken to be 45%. The Z° mass is assumed to be 92.5 GeV. The corresponding uncertainty on $\sin^2\theta_w$ and on M_Z is shown on the right-hand scales. The three branches of the A_{LR} curve refer to the precision of the polarization monitoring. From top to bottom, ΔA_{LR} is shown for $\Delta\mathcal{P}/\mathcal{P} = 5\%$, 3%, and 1%, respectively. A sample of 10^5 to 10^6 events is sufficient to saturate the asymptotic limit, depending upon the precision of the polarization monitoring. The expected uncertainty on $\sin^2\theta_w$ from a measurement of the leptonic forward-backward asymmetry is also shown. The beams are assumed to be unpolarized and the number of muonic decays is assumed to be given correctly by the Standard Model.

2) A layout of the SLAC Linear Collider. The orientation of an electron spin vector is shown as the electron is transported from the electron gun to the interaction point.

3) The band structure of GaAs near the bandgap minimum (from references 2 and 3). The energy levels of the states are shown on the right. Allowed transitions for the absorption of right (left) circularly polarized photons are shown as solid (dashed) arrows. The circled numbers indicate the relative transition rates.

4) The band structure of Gallium Arsenide near its surface[2] for: (a) pure GaAs, (b) GaAs with a cesiated surface, and (c) GaAs with a layer of Cs_2O on its surface.

5) The polarization of electrons emitted from several GaAs photocathodes as functions of photon wavelength. The 0.2 μm and 0.9 μm samples were measured at SLAC by T. Maruyama. The data from Alvarado et al are taken from Reference 5.

6) A drawing of the SLC polarized source. The photoemission source is installed on a Y vacuum section with the thermionic source to facilitate switching from one source to the other. The laser polarization and chopping optics are not shown.

7) The power of the SLC laser is shown as a function of wavelength (which depends upon dye concentration) for two different dyes. The laser power is the time averaged at 60 Hz operation.

8) The modulation and circular polarization optics for the SLC polarized source laser.

9) The spin rotation system as incorporated into the north damping ring complex. The orientation of the polarization vector at several points is shown by the double arrow.

10) The unpolarized differential cross sections for Møller and Bhabha scattering are presented as a function of the center-of-mass scattering angle. The longitudinal and transverse asymmetry functions for both processes are also shown.

11) The beam's eye view of a Møller scattering target to be used at SLC. A holder containing four iron foils can be moved through the beam. Two foils are transverse to the beam and two are tilted at angle of 20° with respect to the beam axis. A set of three Hemholz coils can produce a 100 gauss field along any of the three axes.

12) A schematical representation of a Møller polarimeter for the SLC extraction line.

13) The electron signal as measured in a Møller polarimeter. The top part of the figure shows the number of scattered electrons as a function of scattering angle. The signal appears at the angle that corresponds to the scattered momentum. The background is well described by the Bethe-Heitler process.

14) The unpolarized cross section and the longitudinal and transverse polariza-

tion asymmetries are shown as a function of $x = K'/K'_{max}$ for the scattering of a 2.23 eV photon by a 46 GeV electron (y = 0.389).

15) The location of the SLC Compton polarimeter is shown. A pulse from the laser located on the surface is directed into collision with the electron bea after it has passed through the interaction point.

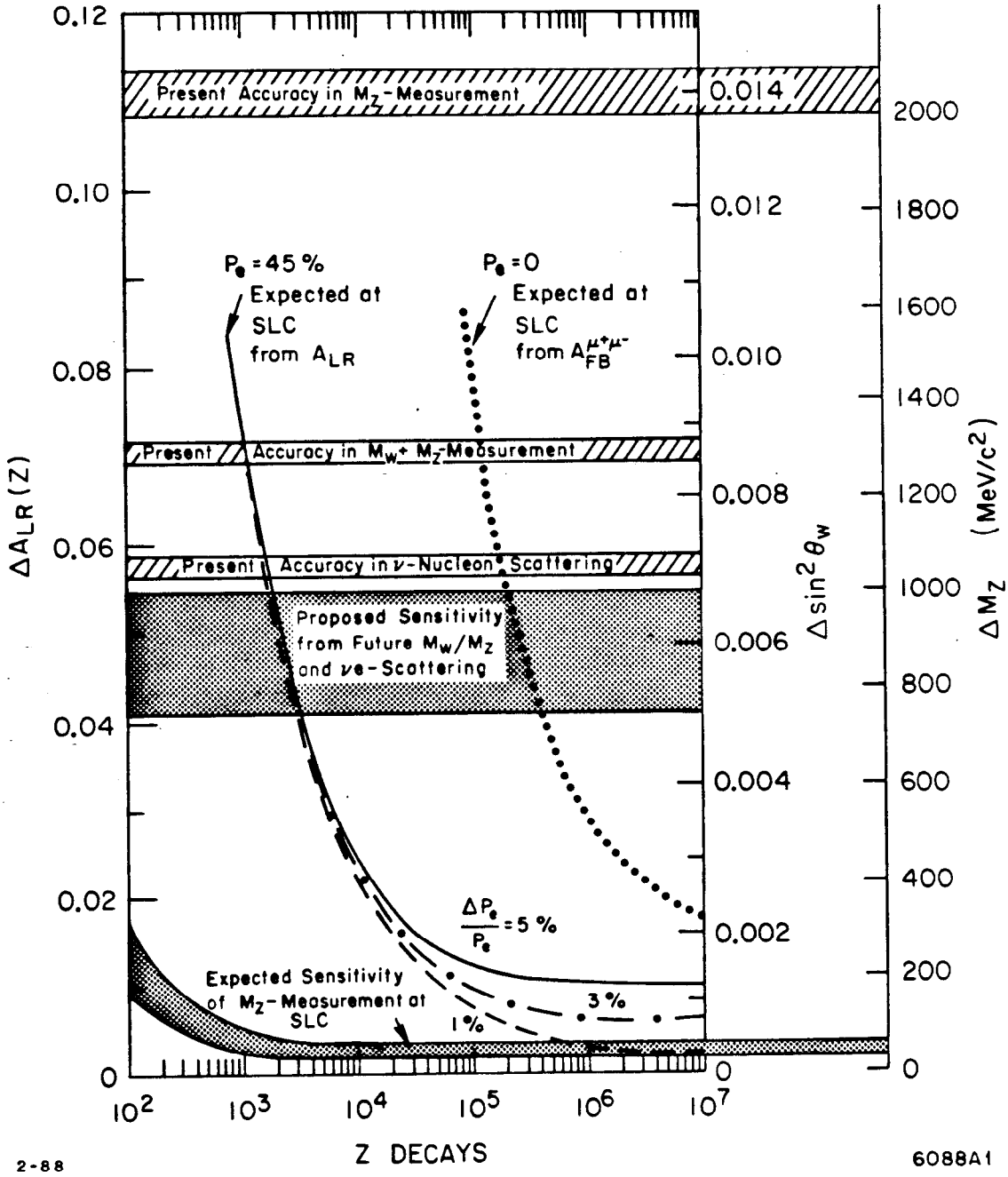
0.12
0.10
0.08
0.06
0.04
0.02
0
ΔA_LR(Z)
Present Accuracy in M_Z-Measurement
0.014
2000
0.012
1800
P_e = 45 %
Expected at
SLC
from A_LR
P_e = 0
Expected at
SLC
from A_FB^μ+μ-
0.010
1600
1400
Present Accuracy in M_W + M_Z-Measurement
0.008
1200
Present Accuracy in ν-Nucleon Scattering
Proposed Sensitivity
from Future M_W/M_Z
and νe-Scattering
0.006
1000
Δsin²θ_W
ΔM_Z (MeV/c²)
800
0.004
600
400
ΔP_e/P_e = 5 %
0.002
200
Expected Sensitivity
of M_Z-Measurement at
SLC
3 %
1 %
0
0
10²
10³
10⁴
10⁵
10⁶
10⁷
Z DECAYS
2-88
6088A1

Fig. 1

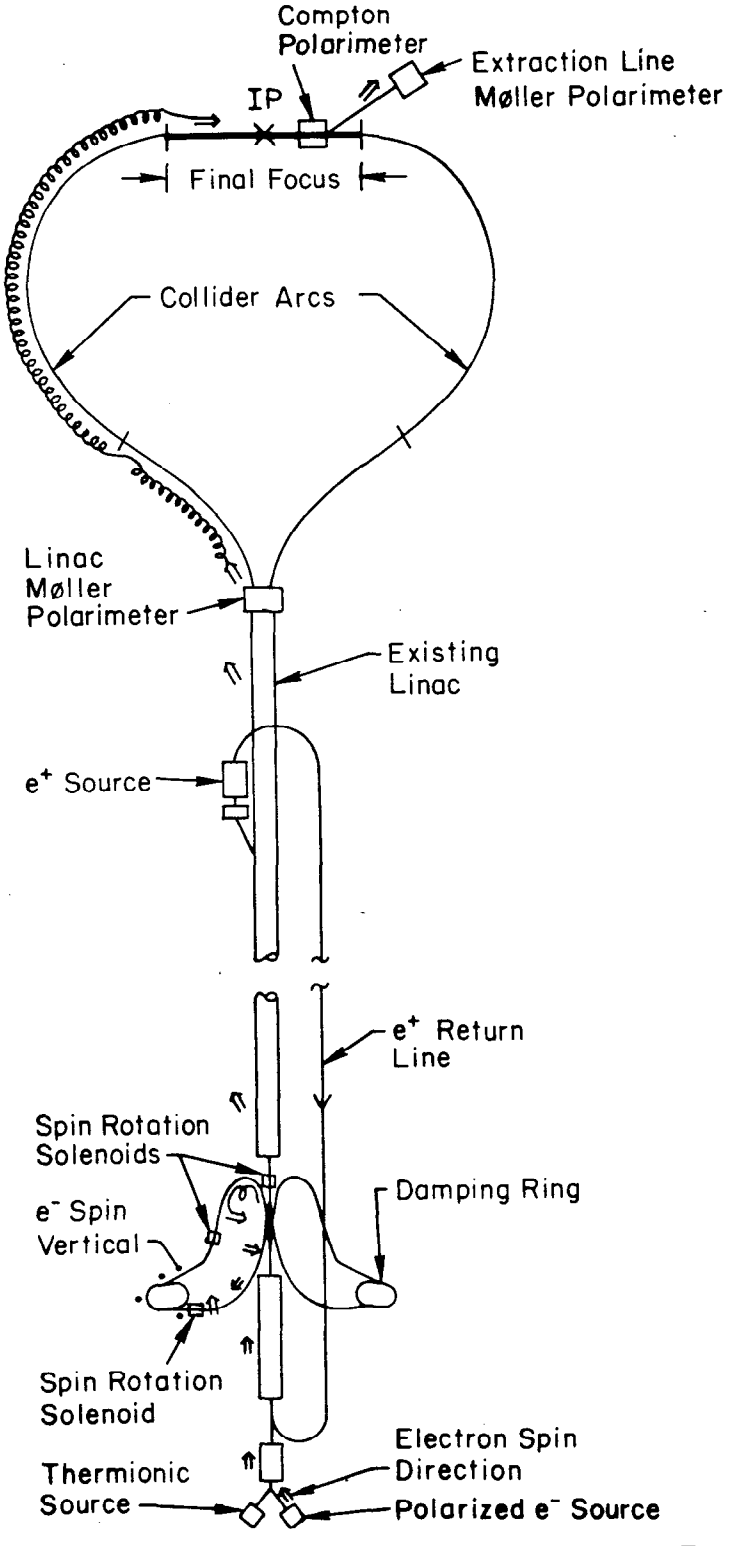
Compton
Polarimeter
Extraction Line
Møller Polarimeter
IP
Final Focus
Collider Arcs
Linac
Møller
Polarimeter
Existing
Linac
e+ Source
e+ Return
Line
Spin Rotation
Solenoids
Damping Ring
e- Spin
Vertical
Spin Rotation
Solenoid
Electron Spin
Direction
Thermionic
Source
Polarized e- Source
POLARIZATION IN THE OVERALL SLC LAYOUT
10-86
5571A4

Fig. 2

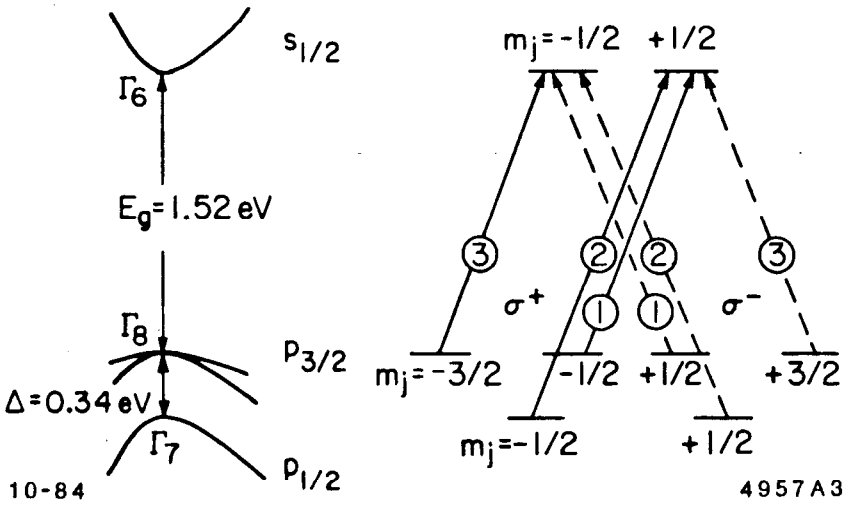
$s_{1/2}$
Γ_6
E_g=1.52 eV
Γ_8
$p_{3/2}$
Δ=0.34 eV
Γ_7
$p_{1/2}$
10-84
m_j=-1/2 +1/2
3
2
2
3
σ+
1
1
σ-
m_j=-3/2
-1/2
+1/2
+3/2
m_j=-1/2
+1/2
4957A3

Fig 3

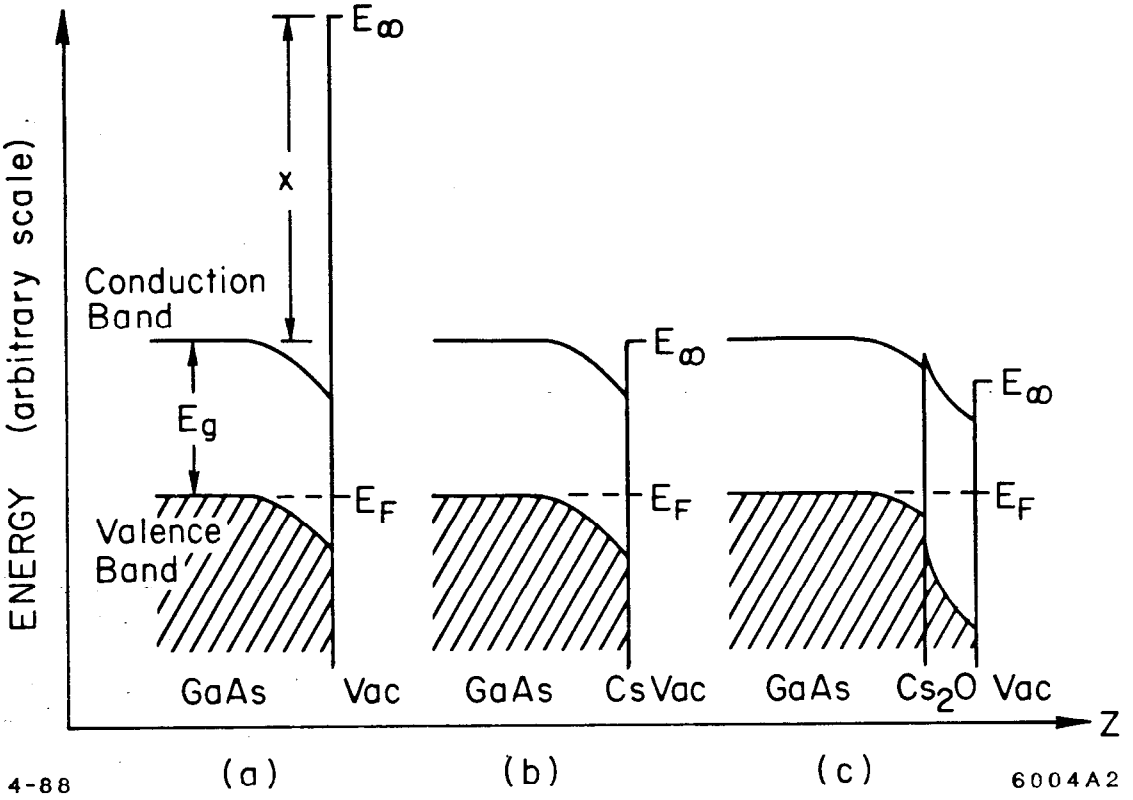
ENERGY (arbitrary scale)
E_∞
x
Conduction Band
E_g
E_F
Valence Band
GaAs
Vac
GaAs
CsVac
GaAs
Cs_2O Vac
Z
4-88
(a)
(b)
(c)
6004A2

Fig. 4

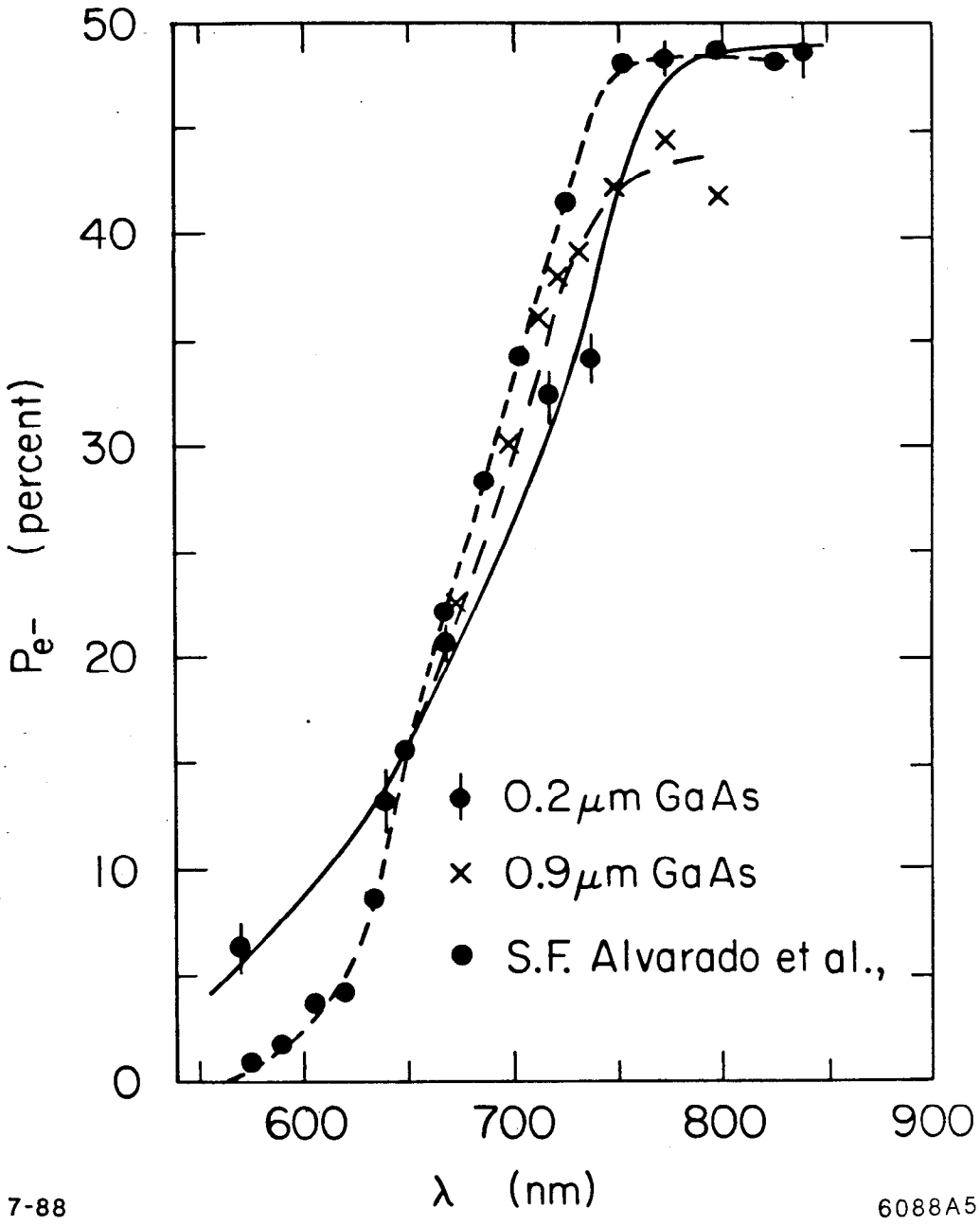
50
40
30
20
10
0
P_{e^-} (percent)
600
700
800
900
λ (nm)
0.2μm GaAs
0.9μm GaAs
S.F. Alvarado et al.,
7-88
6088A5

Fig. 5

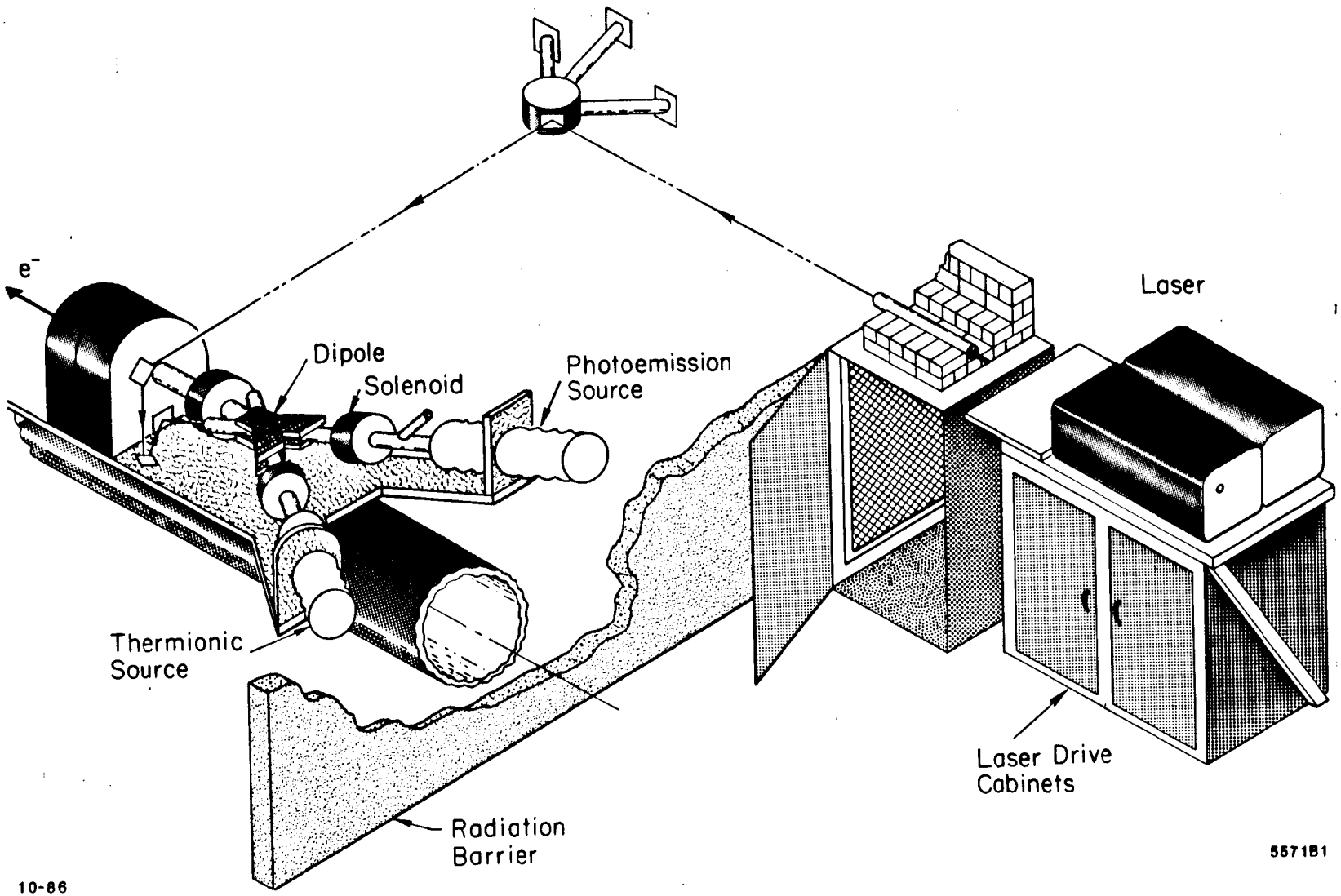
e⁻
Dipole
Solenoid
Photoemission
Source
Laser
Thermionic
Source
Laser Drive
Cabinets
Radiation
Barrier
557181
10-86

Fig. 6

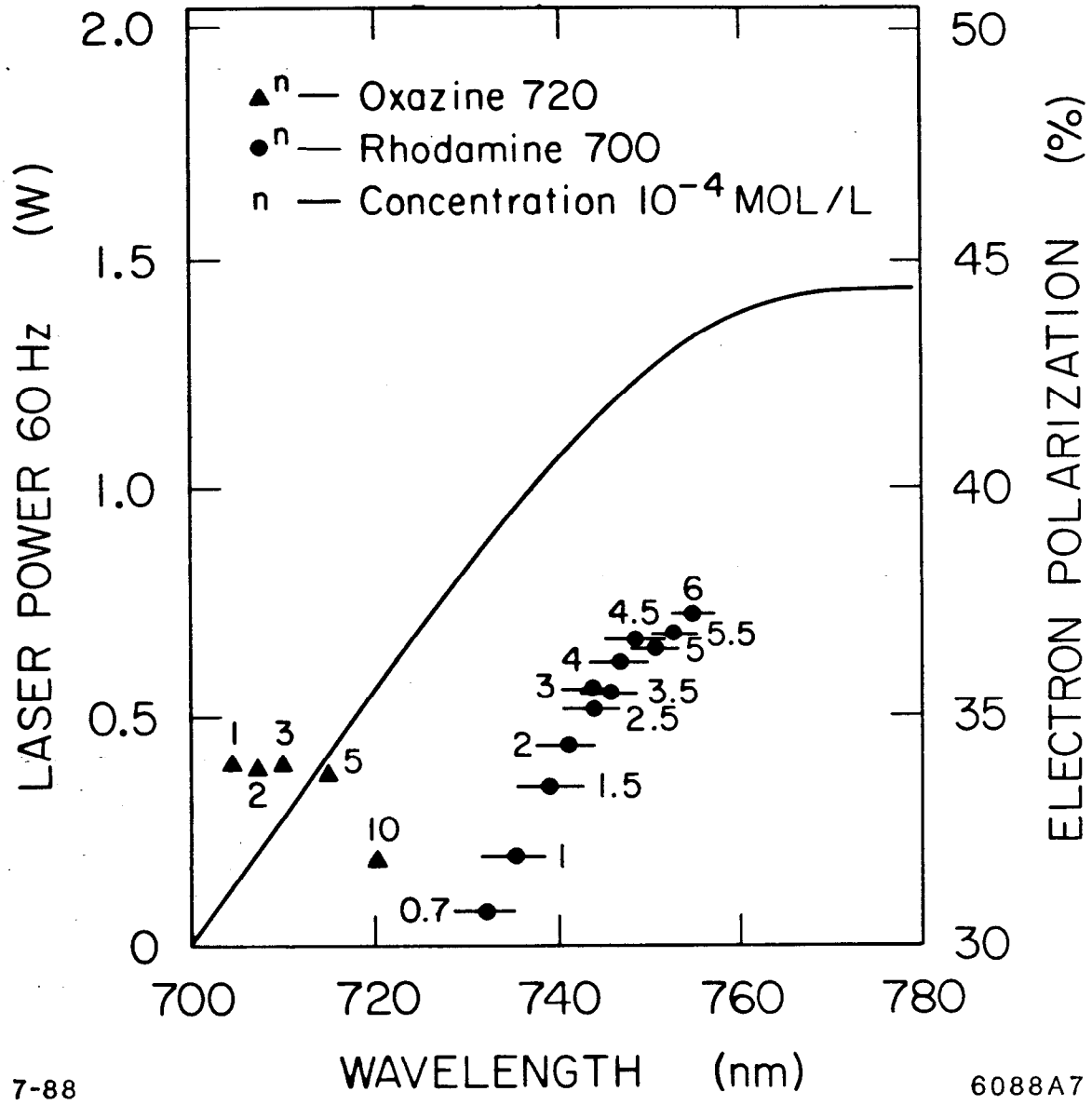
2.0
1.5
1.0
0.5
0
LASER POWER 60 Hz (W)
50
45
40
35
30
ELECTRON POLARIZATION (%)
▲n — Oxazine 720
●n — Rhodamine 700
n — Concentration 10⁻⁴ MOL/L
700
720
740
760
780
WAVELENGTH (nm)
7-88
6088A7

Fig. 7

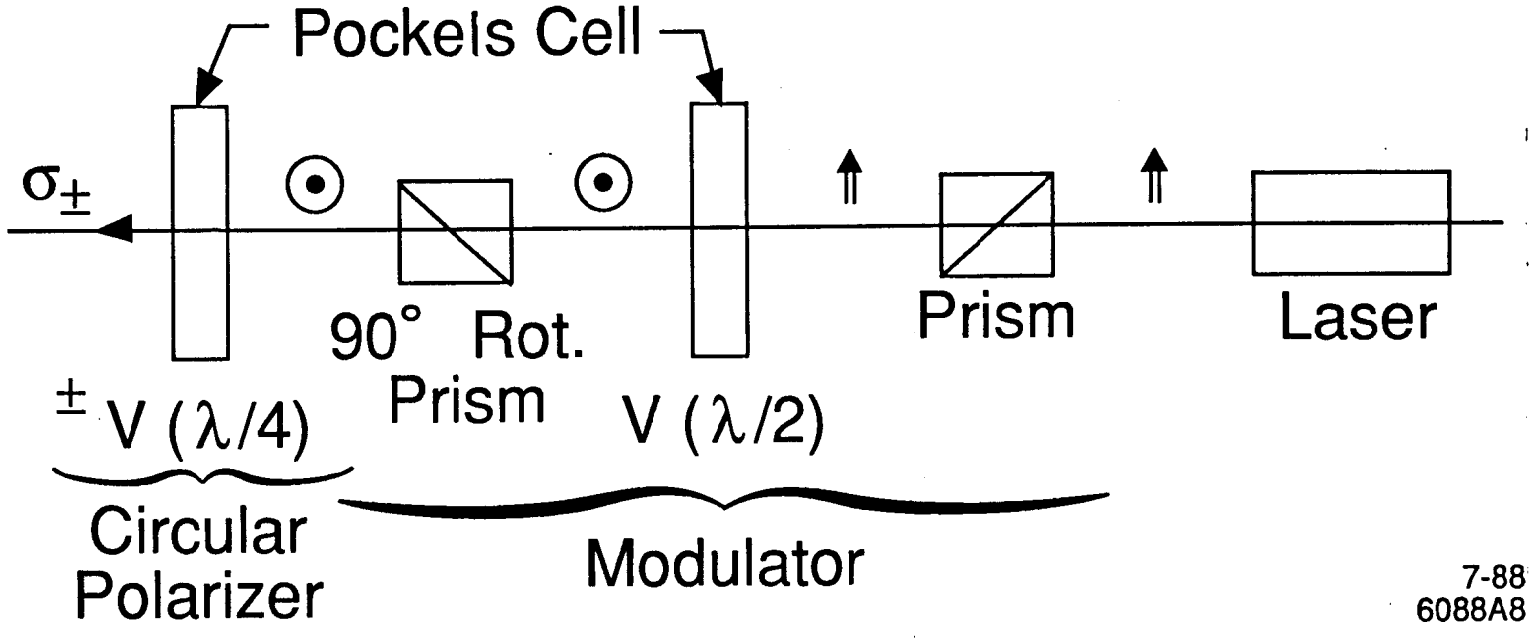
Pockels Cell
$\sigma_{\pm}$
90° Rot. Prism
Prism
Laser
$\pm$ V (λ/4)
V (λ/2)
Circular Polarizer
Modulator
7-88
6088A8

Fig. 8

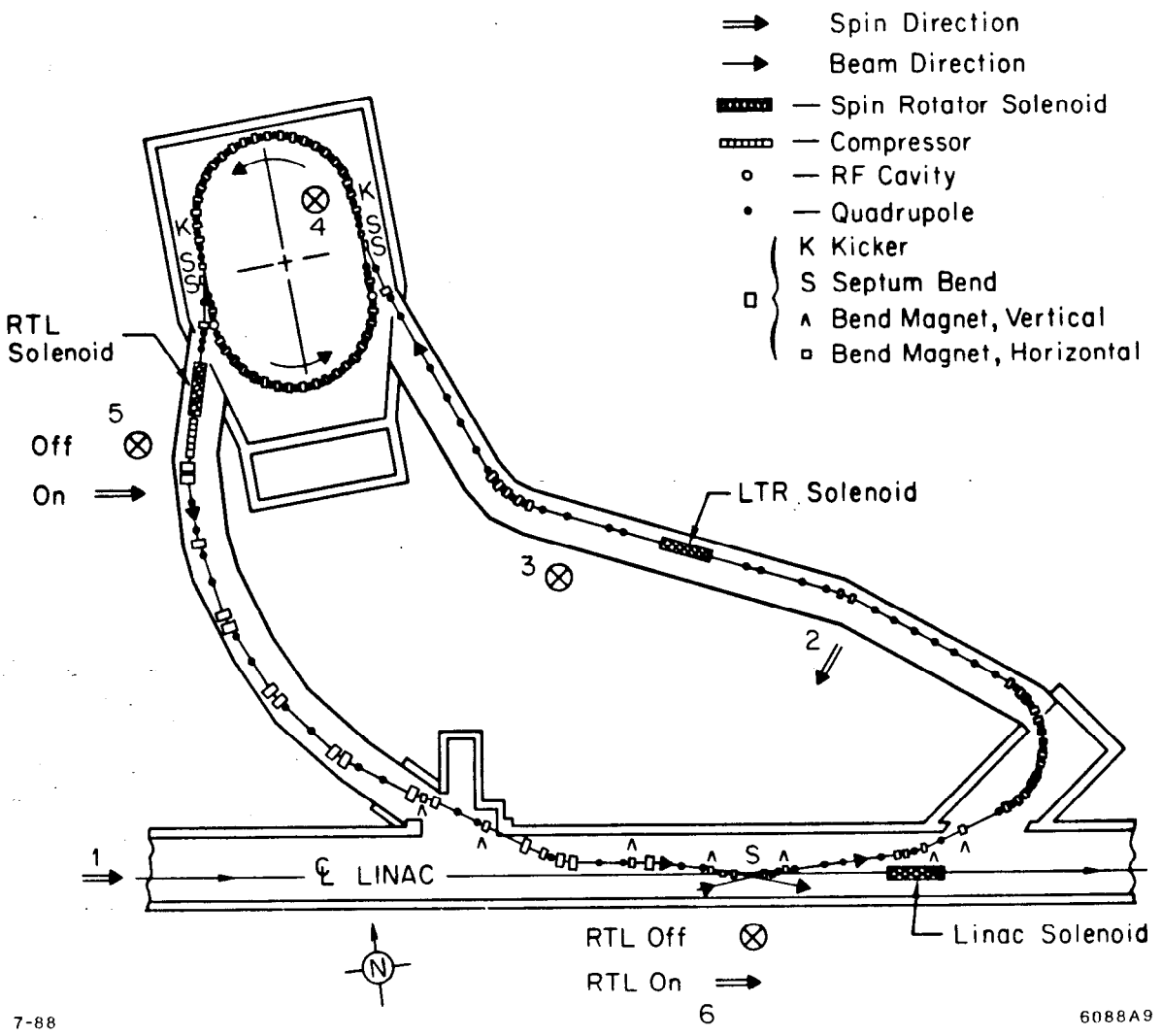
Spin Direction
Beam Direction
Spin Rotator Solenoid
Compressor
RF Cavity
Quadrupole
K Kicker
S Septum Bend
Bend Magnet, Vertical
Bend Magnet, Horizontal
RTL Solenoid
5
Off
On
4
K
S
S
K
S
S
LTR Solenoid
3
2
1
℄ LINAC
S
RTL Off
RTL On
6
Linac Solenoid
N
7-88
6088A9

Fig. 9

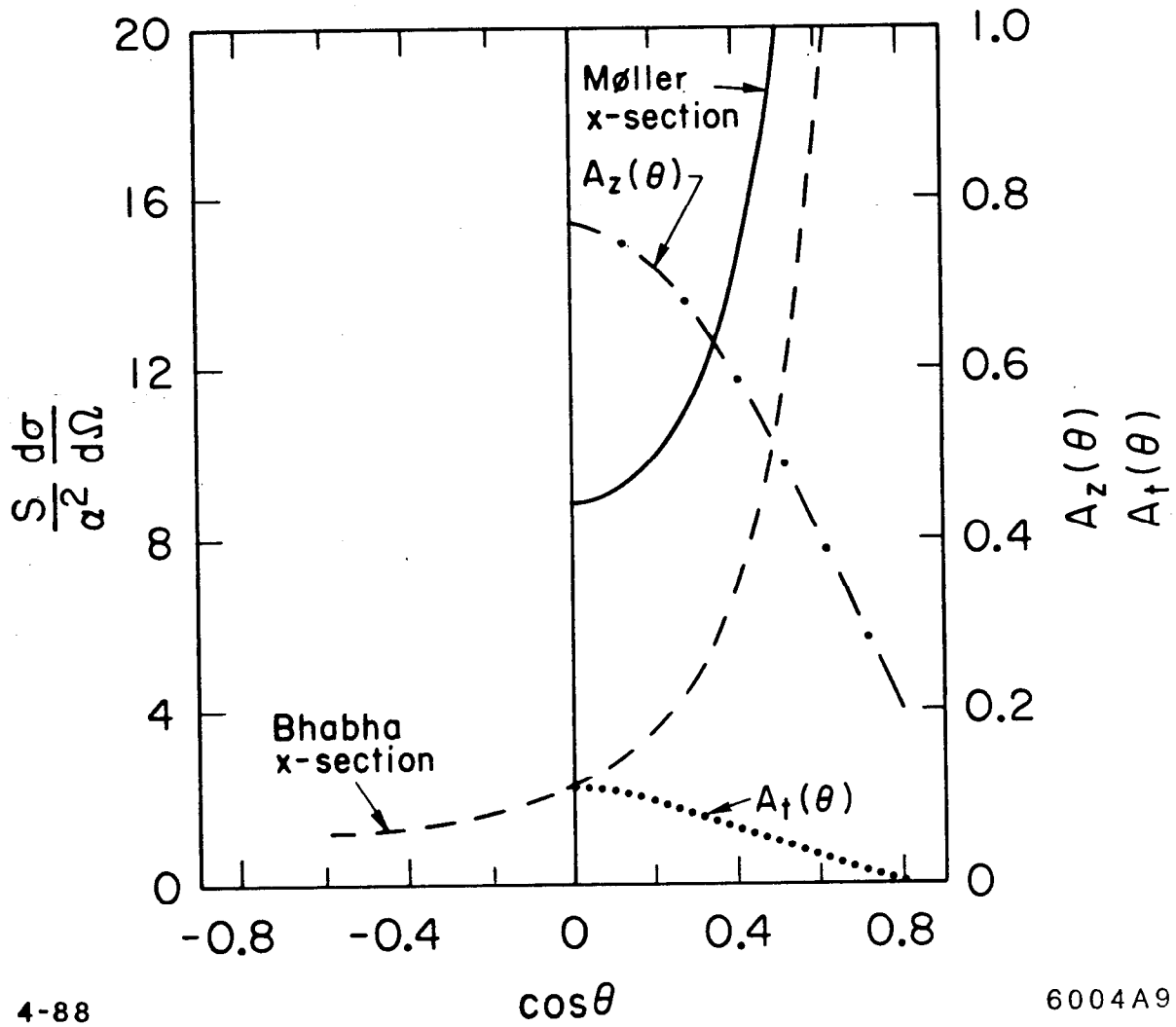
20
16
12
8
4
0
1.0
0.8
0.6
0.4
0.2
0
Møller
x-section
$A_z(\theta)$
Bhabha
x-section
$A_t(\theta)$
$S\left|\frac{d\sigma}{\alpha^2 d\Omega}\right|$
$A_z(\theta)$
$A_t(\theta)$
-0.8
-0.4
0
0.4
0.8
$\cos\theta$
4-88
6004A9

Fig. 10

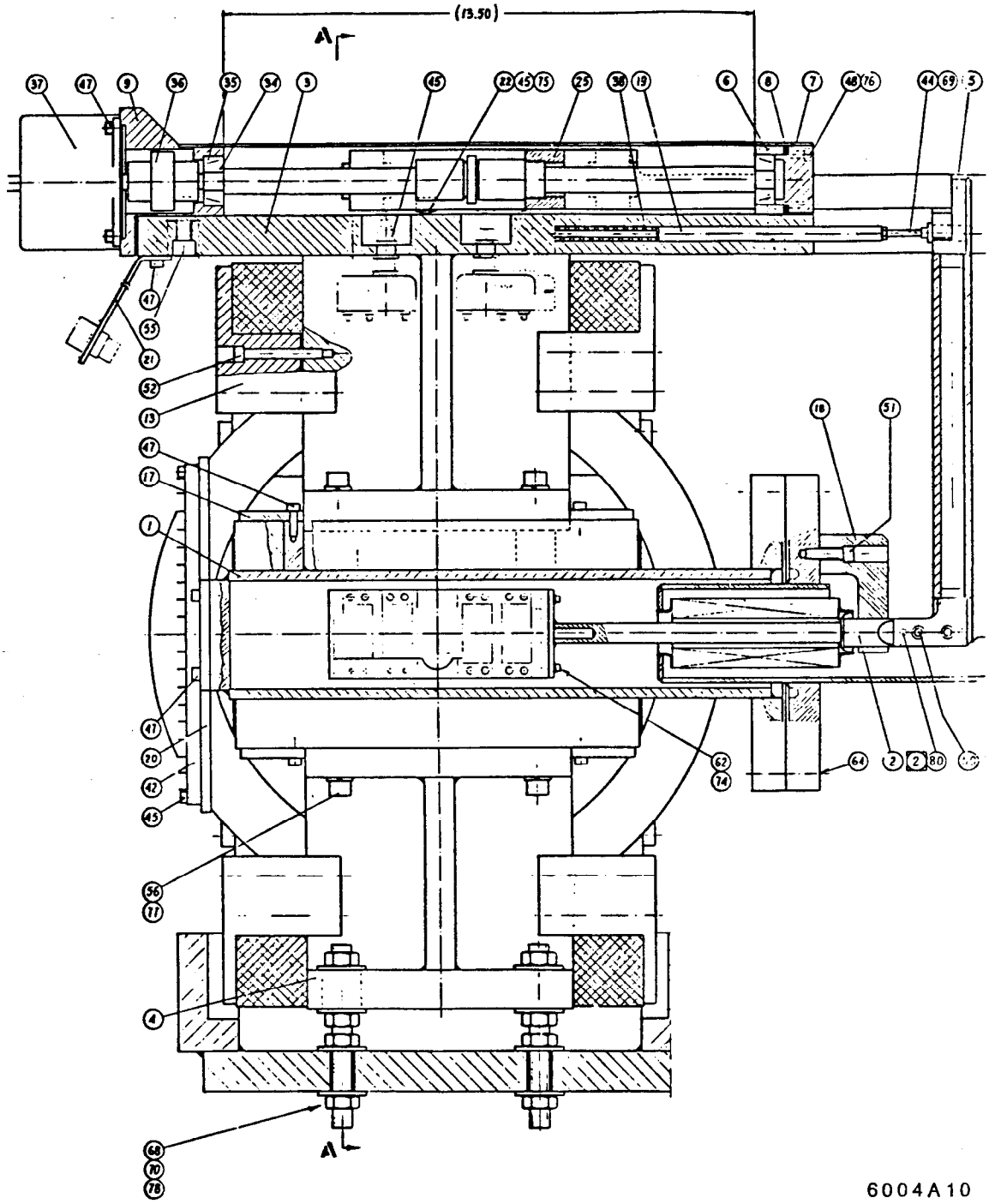

Fig. 11

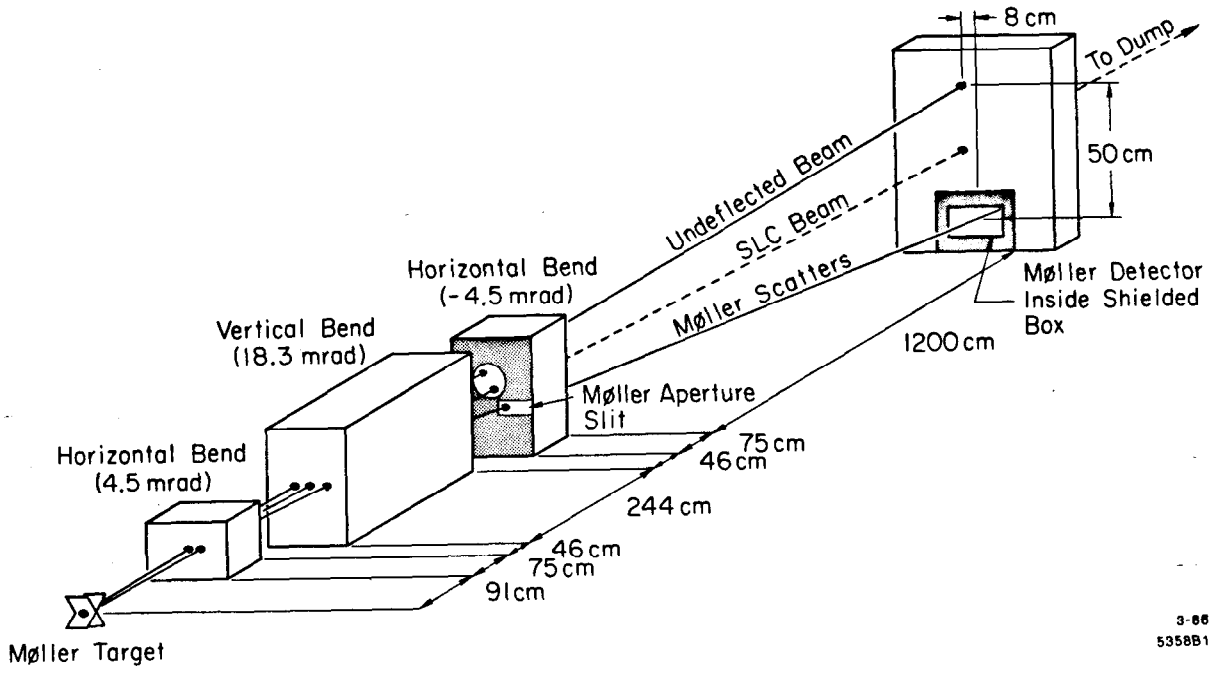
8 cm
To Dump
50 cm
Undeflected Beam
SLC Beam
Møller Scatters
Møller Detector
Inside Shielded
Box
1200 cm
Horizontal Bend
(-4.5 mrad)
Vertical Bend
(18.3 mrad)
Møller Aperture
Slit
75 cm
46 cm
244 cm
Horizontal Bend
(4.5 mrad)
46 cm
75 cm
91 cm
Møller Target
3-86
5358B1

Fig. 12

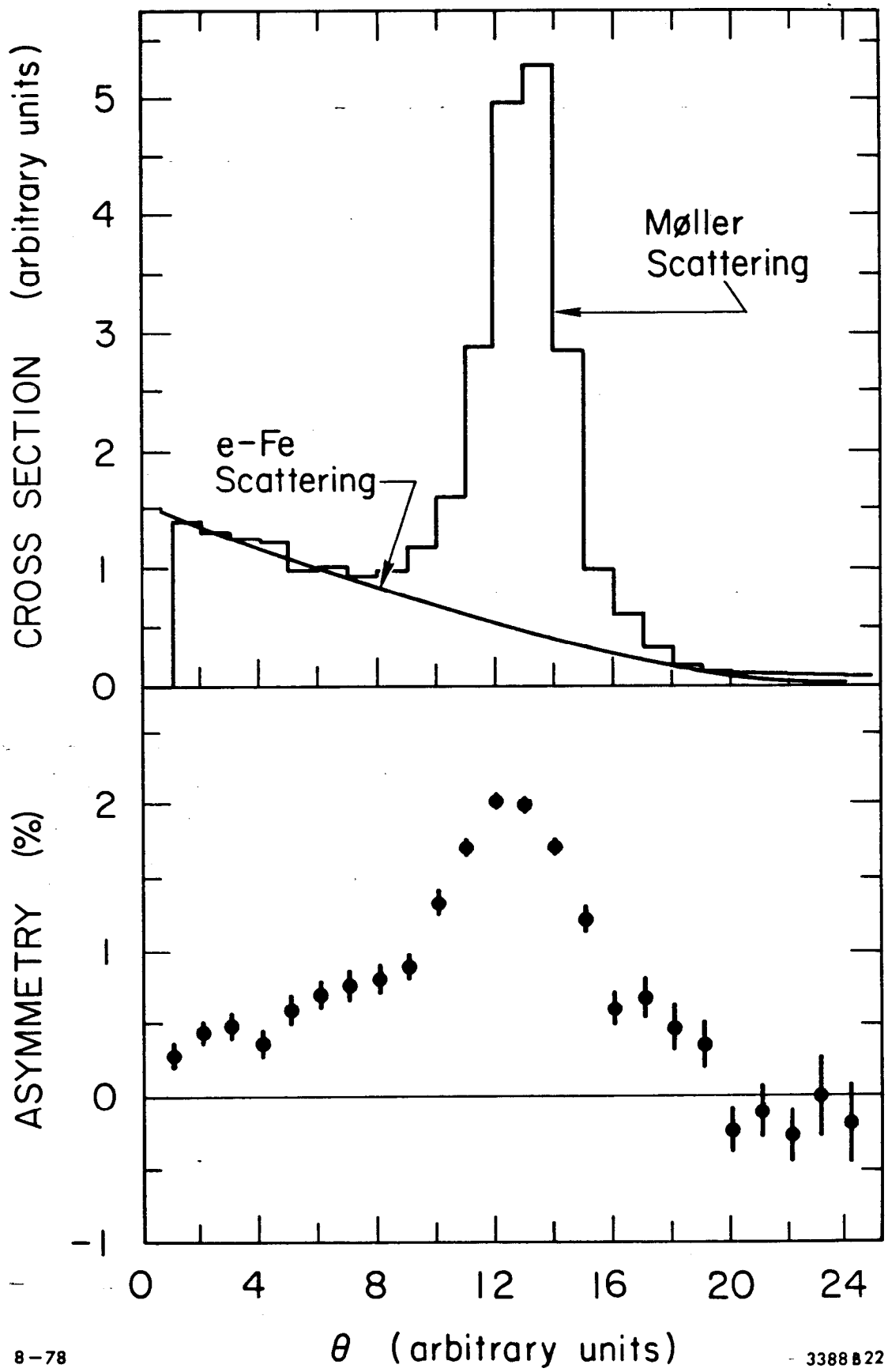
CROSS SECTION (arbitrary units)
5
4
3
2
1
0
Møller
Scattering
e-Fe
Scattering
ASYMMETRY (%)
2
1
0
-1
0
4
8
12
16
20
24
θ (arbitrary units)
8-78
3388B22

Fig. 13

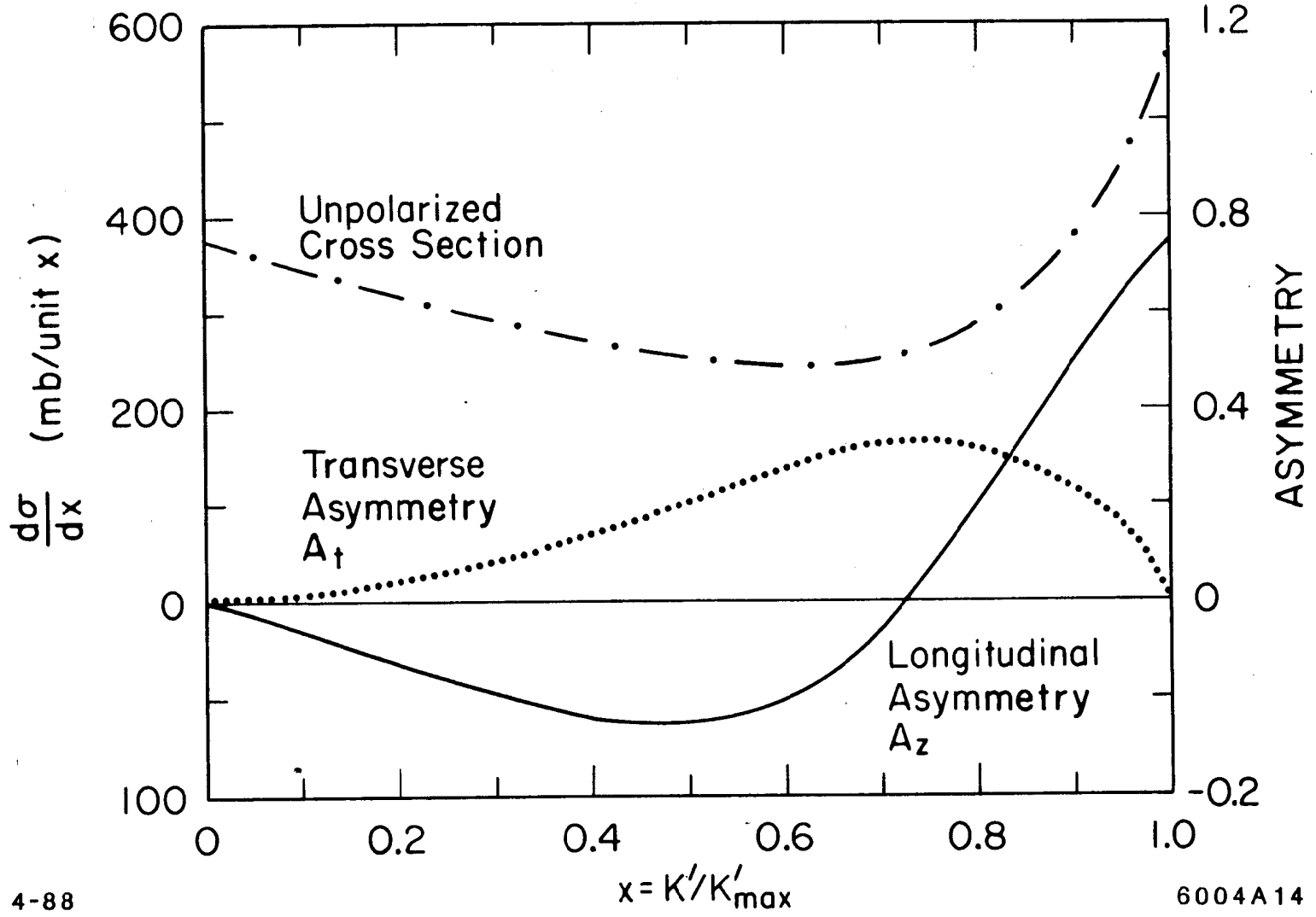
600
400
200
0
100
1.2
0.8
0.4
0
-0.2
0
0.2
0.4
0.6
0.8
1.0
Unpolarized
Cross Section
Transverse
Asymmetry
A_t
Longitudinal
Asymmetry
A_z
$\frac{d\sigma}{dx}$ (mb/unit x)
ASYMMETRY
$x = K'/K'_{max}$
4-88
6004A14

Fig. 14

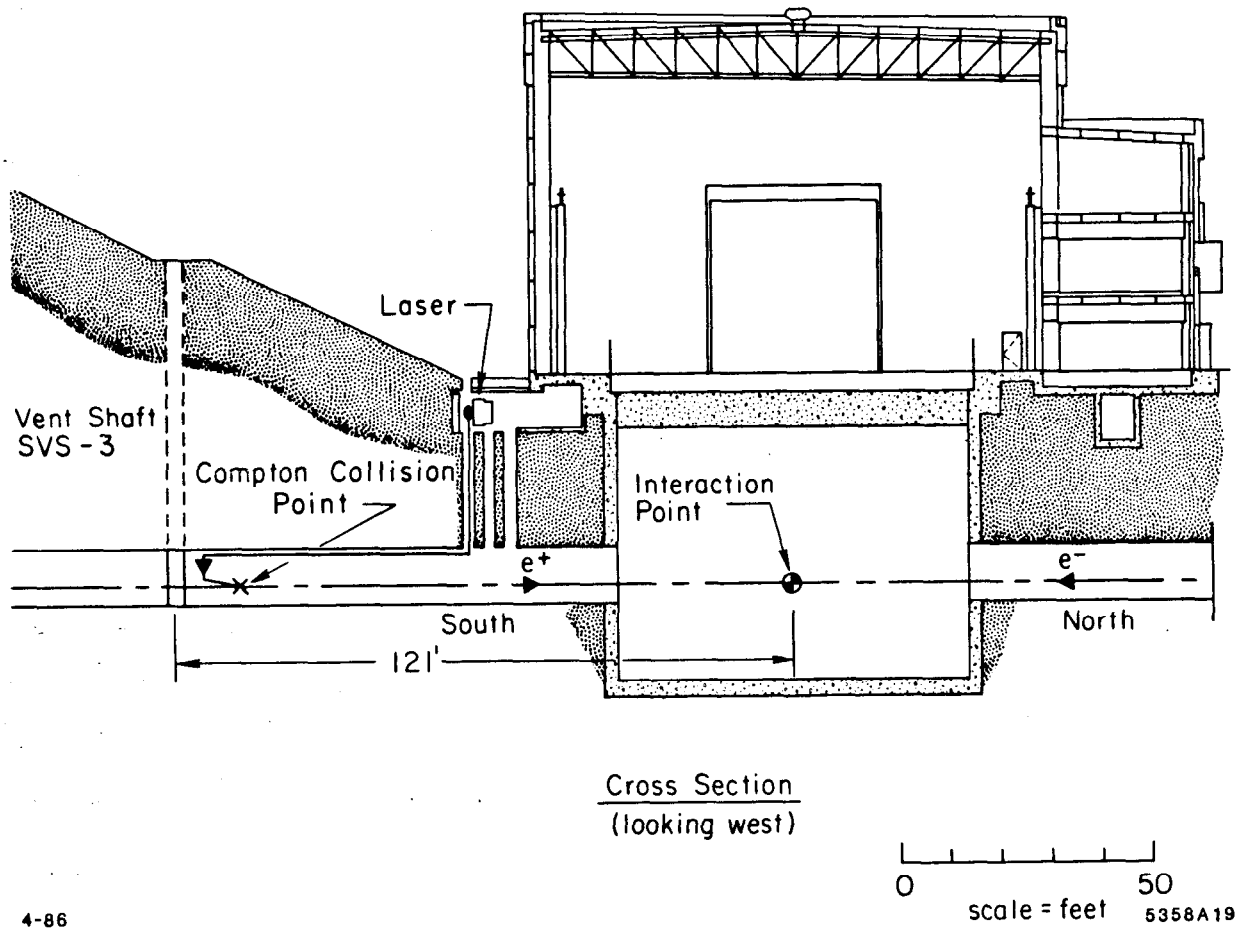
Laser
Vent Shaft
SVS - 3
Compton Collision
Point
Interaction
Point
e+
e−
South
North
121'
Cross Section
(looking west)
0
50
scale = feet
5358A19
4-86

Fig. 15